2017 American Control Conference
Sheraton Seattle Hotel
May 24–26, 2017, Seattle, USA

Hybrid integrator design for enhanced tracking in motion control

D.A. Deenen M.F. Heertjes W.P.M.H. Heemels H. Nijmeijer

Abstract— **This paper discusses a novel hybrid integrator design that (a) gives improved low-frequency disturbance rejection properties under double-integrator control, but (b) avoids the unwanted occurrence of overshoot and settling effects otherwise resulting from adding an extra linear integrator. The main principle behind this new design is that the resulting hybrid element generates a continuous control output signal based on integrator action when possible, while overall satisfying a sector condition that restricts the input-output behavior to a $[0,k_h]$-sector, where k_h is a positive gain derived from a closed-loop stability argument. In fact, closed-loop stability can be guaranteed on the basis of a circle-criterion-like argument and checked through (measured) frequency response data, thereby avoiding the need for parametric models. The strengths of this new hybrid integrator will be demonstrated experimentally on a wafer stage system of an industrial wafer scanner.**

I. Introduction

In this paper, a hybrid integrator design is proposed to cope with the classical trade-off between (a) enhanced low-frequency disturbance suppression as a result of using integral control, and (b) the transient response that often deteriorates by such control [9], [15]. This trade-off generically arises in high-precision mechatronics and in this paper will be particularly discussed in the context of the control of wafer scanners, which are the lithography machines [4] used in the production of microchips that require nanometer accuracies under aggressive motion.

Over the last decades, nonlinear control for (linear) motion systems has been proposed by many researchers, see, for example, [1], [2], [8], [16], [20] and the references therein, as a viable solution to deal with the above-mentioned trade-off. Motivating examples include reset control, see for instance the Clegg integrator that later developed into the first-order reset element (FORE) [6], [7], [11], [13]. The Clegg integrator is a simple integrator that resets its state to zero upon zero input crossings. A slightly modified version, but with the same rationale, was discussed in [18] and is described in state-space form by

$$\mathscr{R}:\begin{cases} \dot{x}_r(t)=\omega_r e(t), & \text{if } e(t)u_r(t)\geq 0 \quad (1a)\\ x_r(t^+)=0, & \text{if } e(t)u_r(t)\leq 0 \quad (1b)\\ u_r(t)=x_r(t), & \quad (1c)\end{cases}$$

with state $x_r\in\mathbb{R}$, input $e\in\mathbb{R}$, output $u_r\in\mathbb{R}$, and integrator frequency $\omega_r\in\mathbb{R}_{\geq 0}$. Through describing function analysis this reset element induces a 20 dB/decade amplitude decay with only 38.15 degrees of phase lag, i.e., a phase advantage of 51.85 degrees compared to a simple linear integrator.

In exploiting this advantage, recently a modified reset integrator design has been proposed in [10], [14], which is similar to (1), but where the flow and jump conditions for the dynamics in (1a) and (1b) are replaced by $eu_r\geq \frac{1}{k_r}u_r^2$ and $eu_r\leq \frac{1}{k_r}u_r^2$, respectively, with k_r a positive-valued gain. Therein, the modified integrator is also experimentally validated and compared to PID- and PI^{2}D-based linear controllers on the motion stages of an industrial wafer scanner. The measurement results clearly demonstrated its benefits, but the resulting performance was somewhat limited by the imposed conditions on closed-loop stability. In fact, input-to-state stability of the closed-loop system with reset is guaranteed by combining a circle-criterion-like argument together with a detectability condition for the reset element. The stability conditions are subsequently assessed by evaluating (measured) frequency response data of the linear part of the closed-loop system in relation to a sector condition that restricts the input-output behavior of the reset element to a $[0,k_r]$-sector. This avoids the need for linear matrix inequality (LMI)-based approaches as in [1], [3], [5], [16], [19] that may be experienced as less insightful in terms of control design and parameter tuning, and, more importantly, require accurate parametric models, which are often non-trivial to obtain in high-precision mechatronics.

In terms of closed-loop performance, i.e., disturbance suppression and transient response, reset-based control as done in [10] may also be limited by higher harmonics induced by the discontinuities in the control signal resulting from resets. That is, the resets distribute low-frequency input energy over a broader frequency interval, including the high-frequency range in which the controlled system is usually more sensitive. To suppress this design limitation, this paper proposes a novel hybrid (yet sector-bounded) integrator design that avoids explicit integrator state resets by moving along the sector bounds when these are reached. As a consequence, the hybrid system switches between an integrator and a gain mode in such a manner that the generated control output is continuous and through sector-boundedness always of equal

This research is supported by the Dutch Technology Foundation STW, carried out as part of the CHAMeleon project "Hybrid solutions for cost-aware high-performance motion control" (no. 13896).

Daniel Deenen is with Eindhoven University of Technology, Department of Mechanical Engineering, Dynamics & Control group, Den Dolech 2, 5600 MB Eindhoven, The Netherlands d.a.deenen@tue.nl

Marcel Heertjes is with ASML, Mechatronics Development, De Run 6501, 5504 DR Veldhoven, The Netherlands marcel.heertjes@asml.com

Maurice Heemels is with Eindhoven University of Technology, Department of Mechanical Engineering, Control Systems Technology group, Den Dolech 2, 5600 MB Eindhoven, The Netherlands m.heemels@tue.nl

Henk Nijmeijer is with Eindhoven University of Technology, Department of Mechanical Engineering, Dynamics & Control group, Den Dolech 2, 5600 MB Eindhoven, The Netherlands h.nijmeijer@tue.nl

sign with the input (error) signal. The latter corresponds to the main philosophy underlying reset control [6]. Additionally, by preserving as much of the integrator buffer as possible instead of instantaneously discarding it through reset, the integrator is found to potentially be more effective in obtaining improved closed-loop performance compared to reset-based integrators.

In line with the above, the main contributions of this paper are (a) the hybrid integrator design, (b) frequency-domain conditions for closed-loop stability that are verifiable using only measured frequency response data, thereby avoiding the need for parametric modeling, and (c) an experimental demonstration of the benefits of the novel design on a wafer stage system of an industrial wafer scanner. The latter will show the hybrid integrator's ability to improve tracking by effectively dealing with the trade-off between low-frequency disturbance suppression and desired transient response.

The remainder of this paper is organized as follows. In Section 2, the hybrid integrator design is discussed in detail. In Section 3, closed-loop stability conditions based on a circle-criterion-like stability argument will be given along with a sketch of the proof. In Section 4, closed-loop stability for a wafer stage system is verified using the conditions presented in the preceding section, and measurement results obtained from experiments on this system are discussed. In Section 5, the main conclusions are summarized.

II. Hybrid Integrator Design

The hybrid integrator-gain system $\mathscr{H}$ (abbreviated as HIGS) is described in state-space form by the switched differential-algebraic equations (DAEs)

$$\mathscr{H}:\begin{cases} \dot{x}_h = \omega_h e, & \text{if } (e,u,\dot{e}) \in \mathscr{F}_1 \quad (2a)\\ 0 = -x_h + k_h e, & \text{if } (e,u,\dot{e}) \in \mathscr{F}_2 \quad (2b)\\ u = x_h & (2c)\end{cases}$$

with state $x_h \in \mathbb{R}$, input $e \in \mathbb{R}$ with corresponding time derivative $\dot{e} \in \mathbb{R}$, control output $u \in \mathbb{R}$, parameters $\omega_h \in [0,\infty)$ and $k_h \in (0,\infty]$ representing the integrator frequency and gain value, respectively, and with $\mathscr{F}_1$ and $\mathscr{F}_2$ denoting the regions in $\mathbb{R}^3$ where the different subsystems are active. $\mathscr{F}_1$ and $\mathscr{F}_2$ will be specified later in such a way that x_h evolves continuously in time. Note that the time evolution of x_h (the value of $\dot{x}_h$) implicitly depends on the derivative $\dot{e}$ of the HIGS' input due to the algebraic constraint in (2b). Indeed, (2b) implies that

$$\dot{x}_h = k_h \dot{e}, \quad \text{if } (e,u,\dot{e}) \in \mathscr{F}_2 \qquad (3)$$

under appropriate smoothness of e. To have well-posed dynamics, we assume the input signal e to be continuous and piecewise differentiable. Also, the initial condition is assumed to be chosen as $x_h(0) = 0$.

Whenever the system evolves according to mode 1 given in (2a) it is said to be in integrator mode. When mode 2 as in (2b) is active, it is referred to as being in gain mode. The switching dynamics are depicted schematically in Fig. 1, where the actual control signals are drawn in solid black

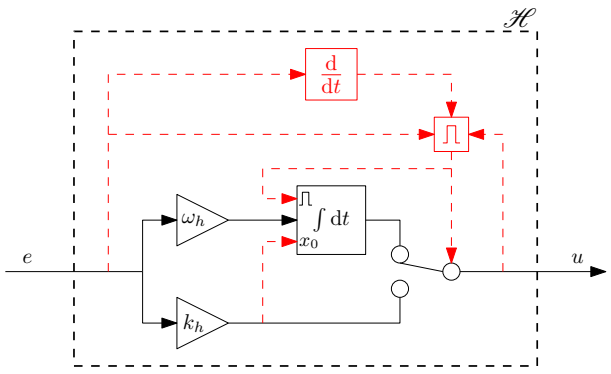

Fig. 1: HIGS according to (2).

and the virtual signals resulting from the implementation of the switching behavior are shown in dashed red. The upper and lower control signal channels yield integrator and gain behavior, respectively, and the switching is determined by the values of e, u, and $\dot{e}$. When the gain mode is active, the value $k_h e(t)$ is continuously passed to the integrator as the initial state value $x_h(t)$ at time t, ensuring that the realized state and output trajectories are continuous when switching back to integrator mode.

The design of the subsets $\mathscr{F}_1$ and $\mathscr{F}_2$ in (2) is based on the desire for the control structure to primarily exhibit the integrator dynamics in (2a), while also having its input-output relation constrained to the sector $[0,k_h]$ illustrated in Fig. 2. The latter is satisfied when it would hold that $(e,u,\dot{e}) \in \mathscr{F}$ at any point in time, where

$$\mathscr{F} := \left\{ (e,u,\dot{e}) \in \mathbb{R}^3 \mid eu \geq \frac{1}{k_h} u^2 \right\}. \qquad (4)$$

To this end, the boundaries of (4) will now be inspected for the integrator dynamics $\dot{x}_h = \omega_h e$ as in (2a). When $u = 0$, all trajectories generated using the integrator dynamics (2a) will remain in $\mathscr{F}$. Indeed, for $u = e = 0$ and arbitrary $\dot{e}$, (2a) yields $\dot{u} = 0$ resulting in trajectories tangential to the plane $u = 0$. Since, additionally, $\ddot{u} = \omega_h \dot{e}$ for this case, the trajectories will remain within $\mathscr{F}$. For $u = 0$, $e \neq 0$ and arbitrary $\dot{e}$, it holds that according to (2a) $\dot{u}$ and e are always of equal sign, implying that all resulting trajectories will travel directly toward the interior of $\mathscr{F}$. However, for certain values of the triple $(e,u,\dot{e})$ on the boundary $u = k_h e$ of

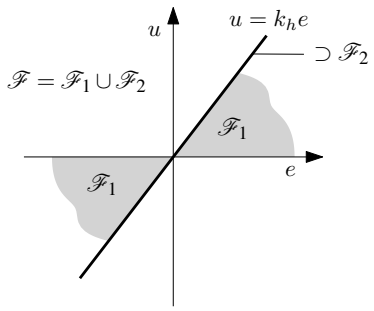

Fig. 2: Schematic representation of the sector $\mathscr{F}$ and the two flow sets $\mathscr{F}_1$ and $\mathscr{F}_2$ in the (e,u)-plane.

$\mathscr{F}$, using the integrator dynamics in (2a) would result in an immediate violation of the sector constraint. Specifically, provided $u = k_h e$, this would occur whenever $\omega_h e > k_h \dot{e}$ for $e > 0$, or when $\omega_h e < k_h \dot{e}$ for $e < 0$, resulting in the overall quadratic condition $\omega_h e^2 > k_h \dot{e} e$. To prevent this, a switch to the gain mode (2b) is then enforced. In particular, $\mathscr{F}_1$ is the subset of $\mathscr{F}$ in which the integrator mode is active, and the set for which the dynamics in (2b) are used to ensure sector-boundedness is denoted by $\mathscr{F}_2$. Given the above observations, the resulting sets governing the active dynamics are thus defined by

$$\mathscr{F}_1 := \mathscr{F} \setminus \mathscr{F}_2, \tag{5a}$$

$$\mathscr{F}_2 := \left\{ (e,u,\dot{e}) \in \mathscr{F} \mid u = k_h e \wedge \omega_h e^2 > k_h \dot{e} e \right\}. \tag{5b}$$

The behavior of the control structure is best illustrated by its response u to a multi-sine input e as depicted in Fig. 3. The injected input signal is given by $e(t) = \sin(t) + 0.5\sin(3t)$ for $t \in \mathbb{R}_{\geq 0}$ and the parameters of the HIGS are set to $\omega_h = 1$ rad/s and $k_h = 1.5$. Initially, the system is in integrator mode, generating the output denoted by $u_{\mathscr{F}_1}$ (red line). When the maximum admissible output $u = k_h e$ (boundary of $\mathscr{F}$) is reached, the HIGS switches to gain mode (green dot) and generates $u_{\mathscr{F}_2}$ (green line) moving along the sector boundary until $(e,u,\dot{e})$ is such that the integrator dynamics would no longer result in a violation of the sector constraint, allowing the switch back to integrator mode (red dot). In Fig. 3c this switch is shown to indeed lie on the boundary $\omega_h e = k_h \dot{e}$ on the plane $u = k_h e$. The system then continues in integrator mode, again followed by a switch to gain mode when necessary, and so on. Note that, contrary to a linear integrator, the HIGS' input and output are always of equal sign, implying that the generated additional control effort is always such that it aids in pushing the system toward zero error. This philosophy is similar to that underlying the design of the Clegg integrator or generalizations like FORE [3], but with the difference that the HIGS generates a continuous control signal, and thereby reduces the undesired excitation of higher harmonics. Also, by switching to the gain mode, the HIGS preserves as much of the integrator buffer as possible without violating the sector constraint, as opposed to discarding it instantaneously though reset. As such, the HIGS has more control authority compared to the reset integrator in [10], [14], enabling it to potentially be more effective in improving closed-loop performance. This is especially true for low values of k_h and k_r, which may be required to guarantee stability, as will be shown in Section 3.

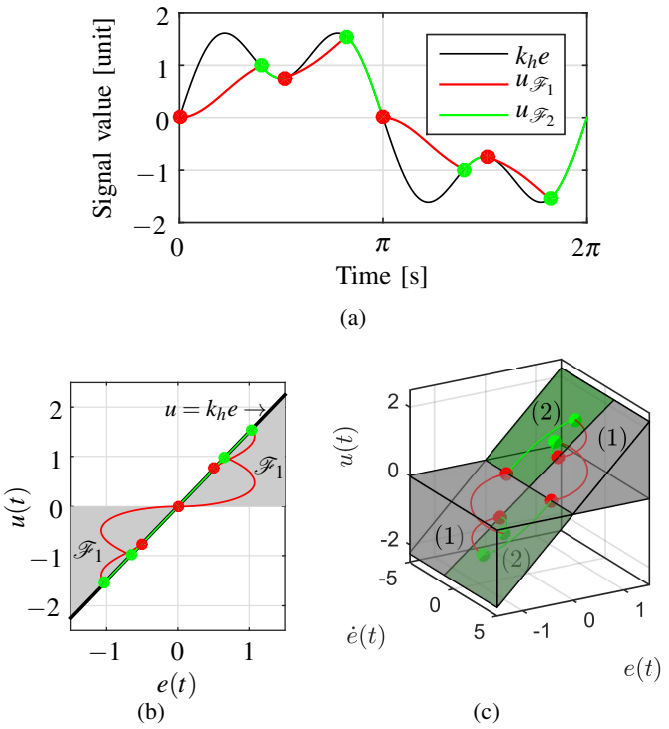

Fig. 3: The time-series response of the HIGS to a multi-sine input with $\mathscr{F}_1$, $\mathscr{F}_2$ in Fig. 3(c) indicated by (1), (2), respectively.

The reduced higher-harmonic excitation becomes apparent from Fig. 4 when comparing the (individually normalized) frequency-domain power distributions of the steady-state outputs generated by (a) a simple (linear) integrator (dashed black), (b) a HIGS (red), and (c) a Clegg integrator (solid black) when subjected to the same sinusoidal input. By avoiding discontinuous output trajectories, the HIGS is able to preserve more output power at the fundamental frequency compared to the Clegg integrator, paving the way for significant performance enhancement due to reduced high-frequency distortion.

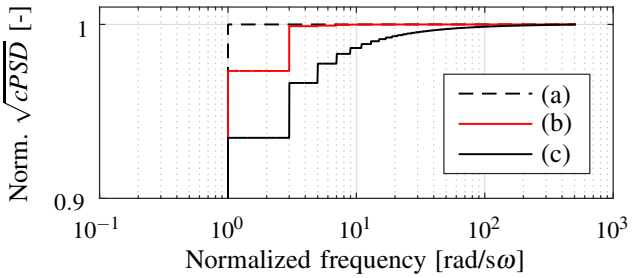

Fig. 4: A comparison of the power distribution over the higher harmonics of the steady-state outputs of (a) a linear integrator, (b) a HIGS, and (c) a Clegg integrator.

III. Frequency-Domain Stability Analysis

Consider the HIGS in the motion control context of Fig. 5. Herein the linear time-invariant (LTI) plant $\mathscr{P}$ with output y_p is controlled by a nominal LTI feedback controller $\mathscr{C}_{nom}$

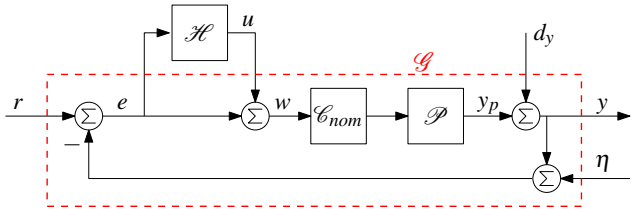

Fig. 5: A representative motion control context featuring the HIGS, indicating the separation of the nonlinear HIGS $\mathscr{H}$ and the linear part $\mathscr{G}$ of the closed-loop system.

and the HIGS $\mathscr{H}$. The output $y = y_p + d_y$ also includes the output disturbance d_y. The inputs to $\mathscr{C}_{nom}$ and $\mathscr{H}$ are, respectively, $w = u + e$ with u the output of the HIGS, and the error signal $e = r - y - \eta$ with the reference signal r and measurement noise η. The linear part of the closed-loop system is denoted by $\mathscr{G}$ (red dashed box). For the ease of presentation, it should be mentioned that feedforward control, which does not affect the upcoming closed-loop stability analysis, has been omitted from the figure. All experimental results presented in Section 4, however, will include the effect of a mass/snap feedforward controller with delay compensation as being key to achieving tracking performance.

Consider the closed-loop system from Fig. 5 rearranged into the equivalent Lur'e form as depicted in Fig. 6 and let the resulting double-input single-output linear system $\mathscr{G}$ be given by the minimal state-space representation

$$\mathscr{G}: \begin{cases} \dot{x}_p = A_g x_p + B_g v + B_{g,\xi}\xi, & \text{(6a)} \\ e = C_g x_p + D_g v + D_{g,\xi}\xi, & \text{(6b)} \end{cases}$$

with states $x_p \in \mathbb{R}^{n_p}$, collected exogenous input $\xi := r - \eta - d_y \in \mathbb{R}$ and input $v := -u \in \mathbb{R}$ generated by the HIGS, and output $e \in \mathbb{R}$. The corresponding transfer functions are given by $\mathscr{G}(s) := [\mathscr{G}_{ev}(s), \mathscr{G}_{e\xi}(s)]$ with

$$\begin{aligned} \mathscr{G}_{ev}(s) &:= C_g(sI_{n_p} - A_g)^{-1}B_g + D_g = \frac{\mathscr{P}(s)\mathscr{C}_{nom}(s)}{1 + \mathscr{P}(s)\mathscr{C}_{nom}(s)}, \\ \mathscr{G}_{e\xi}(s) &:= C_g(sI_{n_p} - A_g)^{-1}B_{g,\xi} + D_{g,\xi} \\ &= \frac{1}{1 + \mathscr{P}(s)\mathscr{C}_{nom}(s)}, \end{aligned} \tag{7}$$

which may be recognized as the complementary sensitivity and sensitivity functions of the nominal control system, respectively. The input-output relation of the HIGS is known to be captured within the sector $[0, k_h]$ by construction, allowing the application of the circle criterion. However, the classical circle criterion does not suffice since the nonlinearity under consideration is a dynamical system, as opposed to being a memoryless nonlinearity typical for Lur'e systems. Therefore, to prove input-to-state stability of the entire control system, an additional invertibility condition on the HIGS' output matrix is adopted to guarantee internal stability of the HIGS, resulting in a similar modification to the circle criterion as proposed by [10], [14].

In order to appropriately formulate the stability conditions corresponding to a Lyapunov-based proof, a SISO representation of $\mathscr{H}$ using only ODEs will be used, given by

$$\mathscr{H}: \begin{cases} \dot{x}_h = \begin{cases} \omega_h e =: \tilde{A}_h x_h + \tilde{B}_{h,1} e, & \text{if } (e,u,\dot{e}) \in \mathscr{F}_1 \\ k_h \dot{e} =: \tilde{A}_h x_h + \tilde{B}_{h,2} e, & \text{if } (e,u,\dot{e}) \in \mathscr{F}_2 \end{cases} \\ u = x_h \quad =: \tilde{C}_h x_h. \end{cases} \tag{8}$$

Note that the dynamics of the gain mode require the explicit use of the time derivative $\dot{e}$. To be able to formulate a SISO state-space representation with only e as input, the derivation with respect to time is (with some abuse of notation) incorporated into $\tilde{B}_{h,2} := k_h \mathrm{d}/\mathrm{d}t$. Although the considered $\mathscr{H}$ is SISO and its state $x_h \in \mathbb{R}$ is only scalar, for generality the representation above is in matrix form to facilitate the extension of the following theorem to the higher-dimensional and multivariable case.

Before presenting the main theorem, consider first the following definition regarding input-to-state stability [12]:

Definition 1: The closed-loop hybrid system as in Fig. 6 with $\mathscr{G}$ as in (6) and $\mathscr{H}$ as in (8) is said to be input-to-state stable (ISS) if there exist a $\mathscr{KL}$-function β and a $\mathscr{K}$-function γ such that for any initial state $x(0)$ with $x_h(0) = 0$ and any bounded, continuous, piecewise differentiable input $\xi : \mathbb{R}_{\geq 0} \to \mathbb{R}$, the corresponding solution $x : \mathbb{R}_{\geq 0} \to \mathbb{R}^n$ satisfies for all $t \in \mathbb{R}_{\geq 0}$

$$\|x(t)\| \leq \beta\left(\|x(0)\|, t\right) + \gamma\left(\sup_{0 \leq \tau \leq t} \|\xi(\tau)\|\right). \tag{9}$$

A sufficient condition for ISS of the system at hand is presented in the following theorem.

Theorem 1: Consider the system in Fig. 6 with $\mathscr{G}$ as in (6) and $\mathscr{H}$ as in (8) with fixed $\omega_h \in [0, \infty)$, $k_h \in (0, \infty]$ and where the output matrix $\tilde{C}_h$ is invertible. Then, this system is ISS if the following conditions are satisfied:

1) The system matrix A_g of (6) is Hurwitz;
2) The transfer function $\mathscr{G}_{ev}$ as in (7) satisfies

$$\frac{1}{k_h} + \mathrm{Re}(\mathscr{G}_{ev}(j\infty)) > 0 \tag{10}$$

and

$$\frac{1}{k_h} + \mathrm{Re}(\mathscr{G}_{ev}(j\omega)) > 0 \text{ for all } \omega \in \mathbb{R}. \tag{11}$$

Sketch of proof: The proof is inspired by the circle criterion and the steps proposed in [10], [14]. The technical setup differs though, as the HIGS is structurally different from the reset element used therein. The steps of the proof are as follows:

1) The nonlinear dynamics of the HIGS are disregarded initially; only the sector-boundedness of its input-output pair (e,u) is exploited. This allows for the circle criterion to be employed in order to prove ISS of $\mathscr{G}(s)$ with respect to ξ and to construct a corresponding quadratic ISS Lyapunov function [17] via the Kalman-Yakubovich-Popov lemma.
2) Using the invertibility property of $\tilde{C}_h$ and the resulting detectability of the pair $(\tilde{A}_h, \tilde{C}_h)$, it can be shown that a quadratic Lyapunov-like function can be constructed for the hybrid integrator element (in isolation).

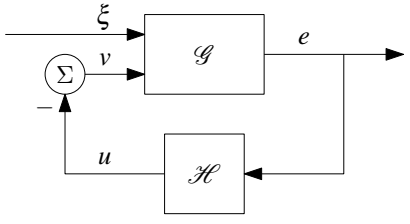

Fig. 6: Closed-loop system in Lur'e form.

3) The Lyapunov functions constructed in the previous two steps are combined and the resulting function is shown to be a (common) quadratic ISS Lyapunov function for the complete closed-loop nonlinear control system, which leads to a bound on the norm of the total state as in (9). ■

Condition 1) of *Theorem 1* can be satisfied by design of a stabilizing nominal feedback controller $\mathscr{C}_{nom}(s)$. Additionally, for motion systems it is typically the case that $\mathscr{G}_{ev}(j\omega) \to 0$ for $\omega \to \infty$, resulting in (10) of condition 2 being satisfied. In such cases, using *Theorem 1* for the closed-loop stability analysis of a HIGS-controlled system thus boils down to the evaluation of (11) of condition 2), which is graphically verifiable using measured frequency response data of $\mathscr{G}_{ev}(s)$ against the known design parameter k_h in a Nyquist diagram. Note that this additionally provides insight regarding robustness margins towards frequency-wise local violation of the condition, which from a practical perspective is highly desirable during the controller design process.

IV. Wafer Stage Measurement Results

As a demonstration of the performance enhancement potential of the HIGS, experiments have been performed on an industrial wafer stage of which the dominant dynamics can be modeled using the transfer function

$$\mathscr{P}(s) = \frac{1}{ms^2} + \frac{-1}{m\left(s^2 + 2\beta_0\omega_0 s + \omega_0^2\right)}, \tag{12}$$

with mass $m = 18$ kg, resonance frequency $\omega_0 = 2\pi 1049$ rad/s, and damping coefficient $\beta_0 = 0.05$. In verifying the stability conditions for the system used for the experiments, condition 1) of *Theorem 1* is satisfied by nominal control design. Condition 2) follows from Fig. 7, which depicts the measured frequency response data of $\mathscr{G}_{ev}$, showing that all $k_h < 0.64$ satisfy the condition. Note that in view of robust stability a robustness margin for k_h, e.g., $k_h < 0.5 \times 0.64$, is advisable. Also note that the choice of ω_h does not play a role in *Theorem 1*. Higher values of k_h, ω_h result in a more aggressive HIGS, which has been observed to improve performance in the low-frequency interval, but reaches an optimum regarding the high-frequency interval. Also, the ratio ω_h/k_h strongly influences closed-loop performance. For lower or higher ratios the dominant dynamics tend increasingly to those of a Clegg integrator or a gain, respectively. A balanced set of parameter values is found at $k_h = 0.3$ and $\omega_h = 200$ rad/s.

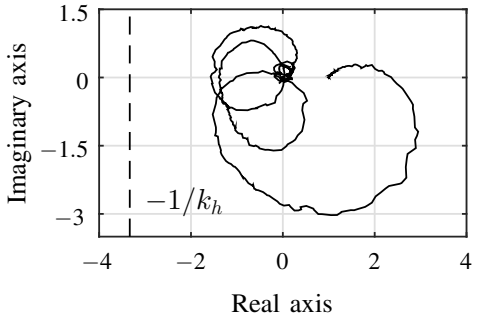

Fig. 7: The Nyquist diagram of $\mathscr{G}_{ev}(s)$ against the value $-1/k_h$ for the graphical verification of the modified circle criterion.

A representative scanning setpoint and a sampling frequency of 20 kHz are used during the experiments. The results obtained when using only the nominal PID-based control design (black) or with additionally the HIGS (red) in the control configuration depicted in Fig. 5 are given in frequency domain in Fig. 8. No results are shown for the linear double-integrator case, since any non-trivial additional linear integrator (performance-wise) caused a violation of the machine's safety margins on the tracking error, resulting in test failure. The figure shows stronger disturbance attenuation in the low-frequency range, but without the high-frequency amplification typically associated with an additional linear integrator as a result of the waterbed effect underlying the Bode sensitivity integral. Overall, an improvement of almost a factor 2 is observed.

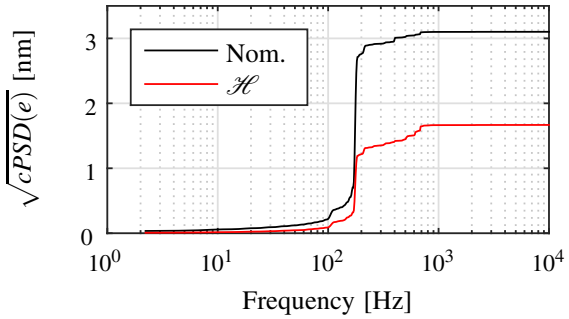

Fig. 8: Cumulative power spectral densities (cPSD) of e.

Time-domain results of four repeated measurements per control configuration are shown in Fig. 9, alongside the (scaled) acceleration profile (dash-dotted black) corresponding to a fourth-order point-to-point motion setpoint. Additionally, the start of the relevant constant-velocity (i.e., zero-acceleration) scanning interval is indicated (dashed black). It can be seen that the HIGS (red) significantly improves disturbance rejection compared to the nominal case (black), while inducing neither the extra overshoot nor the deteriorated settling behavior that with additional linear integral control would inevitably be present. This follows for the unfiltered error signals e, as well as for the filtered signals obtained using either a moving average ($\mathscr{M}_A$) filter or a moving standard deviation ($\mathscr{M}_{SD}$) filter

$$\mathscr{M}_A(e(t)) = \frac{1}{T_e}\int_{t-T_e/2}^{t+T_e/2} e(\tau)\,\mathrm{d}\tau, \tag{13}$$

$$\mathscr{M}_{SD}(e(t)) = \sqrt{\frac{1}{T_e}\int_{t-T_e/2}^{t+T_e/2} \left(e(\tau) - \mathscr{M}_A(e(t))\right)^2 \mathrm{d}\tau}, \tag{14}$$

where T_e denotes the exposure time of a single point on the wafer during scanning. The $\mathscr{M}_A$ filter is basically a low-pass filter providing a good measure on system overlay (the accuracy with which consecutive layers can be stacked in the microchips on the wafer), and the $\mathscr{M}_{SD}$ filter resembles

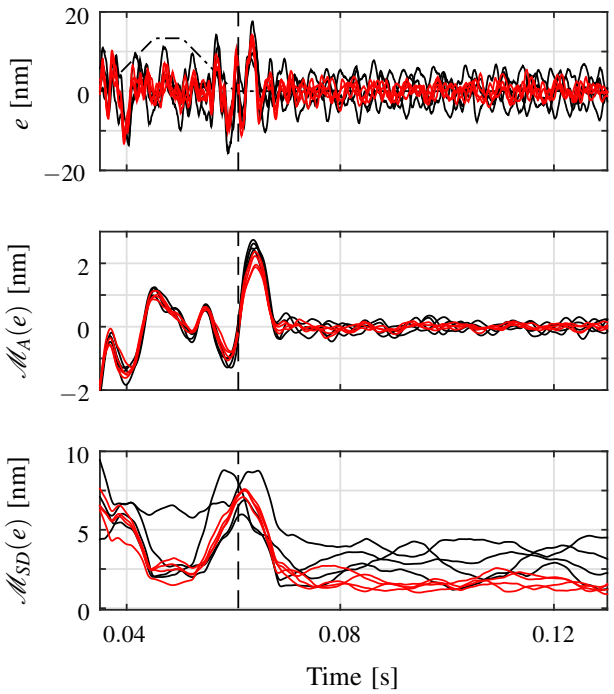

Fig. 9: Time-series measurement of e, $\mathscr{M}_A(e)$, and $\mathscr{M}_{SD}(e)$.

a high-pass filter as to reflect the imaging quality. Note that both Figs. 8 and 9 show hardly any effect of high-frequency distortion due to the continuous switching from gain to integrator mode and vice versa.

V. Conclusions

In this paper a hybrid integrator design (HIGS) is proposed that effectively deals with the traditional trade-off between (a) enhanced low-frequency disturbance suppression as a result of using integral control, and (b) the desired transient response that often deteriorates by such control. Different from (Clegg-based) reset designs that often pursue a similar objective, the HIGS also features enhanced high-frequency performance as a result of the absence of resets, since this strongly limits the excitation of higher harmonics. Stability conditions of the HIGS-based closed-loop system are provided, which can be verified using (measured) frequency response data, thereby avoiding the need for parametric modeling. Experimental results obtained from an industrial wafer stage system demonstrate the effectiveness of the HIGS by improved low-frequency disturbance rejection with neither deteriorated overshoot or settling effects nor high-frequency distortion.

References

[1] W.H.T.M. Aangenent, G. Witvoet, W.P.M.H. Heemels, M.J.G. van de Molengraft and M. Steinbuch, Performance analysis of reset control systems, *International Journal of Robust and Nonlinear Control* (2009).

[2] O. Beker, C.V. Hollot and Y. Chait, Plant with Integrator: An Example of Reset Control Overcoming Limitations of Linear Feedback. *IEEE Transactions on Automatic Control*, vol.46, no.11, 1797-1799 (2001).

[3] O. Beker, C.V. Hollot, Y. Chait and H. Han, Fundamental properties of reset control systems. *Automatica*, vol.40, 905-915 (2004).

[4] H. Butler, Position control in lithographic equipment: an enabler for current-day chip manufacturing. *Control Systems, IEEE*, vol.31, no.5, 28-47 (2011).

[5] J. Carrasco, A. Baños and A. van der Schaft, A passivity-based approach to reset control systems stability. *Systems & Control Letters*, vol.59, 18-24 (2010).

[6] Y. Chait and C.V. Hollot, On Horowitz's contributions to reset control. *International Journal of Robust and Nonlinear Control*, vol.12, 335-355 (2002).

[7] J.C. Clegg, A Nonlinear Integrator for Servomechanisms. *Transactions of the A.I.E.E.*, vol.77 (Part II), 41-42 (1958).

[8] A. Feuer, G.C. Goodwin and M. Salgado, Potential Benefits of Hybrid Control for Linear Time Invariant Plants. *Proceedings of the American Control Conference*, 2790-2794 (1997).

[9] J. Freudenberg, R. Middleton, and A. Stefanopoulou, A survey of inherent design limitations. *Proceedings of the American Control Conference*, vol.5, 2987-3001 (2000).

[10] M.F. Heertjes, K.G.J. Gruntjens, S.J.L.M. van Loon, N. van de Wouw, and W.P.M.H. Heemels, Experimental evaluation of reset control for improved stage performance. *IFAC-PapersOnLine 49-13*, 93-98 (2016).

[11] I.M. Horowitz and P. Rosenbaum, Non-linear design for cost of feedback reduction in systems with large parameter uncertainty. *International Journal of Control*, vol.21, no.6, 977-1001 (1975).

[12] H.K. Khalil. (2002) Nonlinear systems, Third edition, Prentice hall, Upper Saddle River.

[13] K.R. Krishnan and I.M. Horowitz, Synthesis of a non-linear feedback system with significant plant-ignorance for prescribed system tolerance. *International Journal of Control*, vol.19, no.4, 689-706 (1974).

[14] S.J.L.M. van Loon, K.G.J. Gruntjens, M.F. Heertjes, N. van de Wouw, and W.P.M.H. Heemels, Frequency-domain tools for stability analysis of reset control systems. Accepted for publication in *Automatica* (2017).

[15] R.H. Middleton, Trade-offs in Linear Control System Design. *Automatica*, vol.27, no.2, 281-292 (1991).

[16] D. Nešić, L. Zaccarian and A.R. Teel, Stability properties of reset systems. *Automatica*, vol.44, 2019-2026 (2008).

[17] E.D. Sontag, On the input-to-state stability property. *European Journal of Control*, vol.1, 24-36 (1995).

[18] L. Zaccarian, D. Nešić and A.R. Teel, First order reset elements and the Clegg integrator revisited. *American Control Conference* (2005).

[19] L. Zaccarian, D. Nešić and A.R. Teel, Analytical and numerical Lyapunov functions for SISO linear control systems with first-order reset elements. *International Journal of Robust and Nonlinear Control*, vol.21, 1134-1158 (2011).

[20] Y. Zheng, Y. Chait, C.V. Hollot, M. Steinbuch and M. Norg, Experimental demonstration of reset control design. *Control Engineering Practice*, vol.8, 113-120 (2000).